Brazilian Journal
of Chemical
Engineering

ISSN 0104-6632
Printed in Brazil
www.scielo.br/bjce

(cc) BY

Vol. 34, No. 04, pp. 1175 – 1189, October – December, 2017
dx.doi.org/10.1590/0104-6632.20170344s20160379

CFD SIMULATION OF THE MIXING AND DISPERSING OF FLOATING PARTICLES IN A VISCOUS SYSTEM

Baoqing Liu[1], Yijun Zheng[1], Mingqiang Chen[1], Xiaoge Chen[1] and Zhijiang Jin[1,*]

[1]Institute of Process Equipment, College of Energy Engineering, Zhejiang University,Hangzhou, 310027, Zhejiang, China
*E-mail: zhijiangjin@126.com; Phone: +86 57187952729,

(Submitted: December 1, 2015; Revised: June 15, 2016; Accepted: August 11, 2016)

Abstract – Based on the Gidaspow model, the distributions of velocity, turbulence intensity, and solid concentration in stirred vessels equipped with a down-pumping propeller (TXL), a six flat-blade disc turbine (Rushton), or a down-pumping six 45° pitched-blade turbine (PBTD-6) in a viscous system were simulated. The power curve of the TXL propeller and the dimensionless solid concentrations of one sampling point in the vessel at different agitation speeds were obtained by simulation and experiment, which were in good agreement with each other. The results showed that: (1) both the tangential velocity and turbulence intensity on the liquid surface caused by a Rushton turbine were the highest of the three conditions at the same agitation speed; (2) the turbulence intensity on the azimuth of 90° behind the baffle near the shaft on the liquid surface was relatively larger than that in other regions; (3) the uniformity of solid concentration distribution in the stirred vessel equipped with a Rushton or PBTD-6 turbine was better than that with a TXL impeller at the same agitation speed.

Keywords: Solid-liquid mixing; Numerical simulation; Computational fluid dynamics (CFD); Impeller type.

INTRODUCTION

Mixing plays a vital role in occasions such as homogenization, emulsification, polymerization and fermentation. The quantity of stirred reactors is more than 85% of the total reactors in the production process of three synthetic materials, namely synthetic plastics, synthetic fiber, and synthetic rubber (Feng and Wang, 2010; Wang and Feng, 2000). In addition to experimental research, computational fluid dynamics (CFD) is gradually becoming an important method in the study of varieties of mixing conditions with the rapid development of the finite volume method and computer technology (Rajavathsacai et al., 2014). Compared with single-phase mixing, solid-liquid mixing is more complicated because of the large density difference between phases. The critical speed, critical power, local velocity and concentration can be conveniently obtained through experiments. But it is hard to obtain the flow pattern and entire concentration distribution in the vessel due to the low efficiency and high cost (Tamburini et al., 2013). Based on this, it is essential to investigate the CFD simulation of solid-liquid mixing.

So far, the simulation studies of solid-liquid mixing focused more on the suspension process of sinking particles. Fan et al.(2005) compared the solid-liquid mixing of slender particles and spherical particles (ρ_s = 1125 kg·m^{-3}) by simulation, and found that the shape of particles had little effect on the velocity field in the vessel equipped with a Rushton turbine. Kasat et al. (2008) simulated the solid-liquid mixing of glass particles in water with a Rushton turbine. They concluded that the mixing time increased with the agitation speed until a peak value and then gradually decreased. It became a constant after getting over the just off-bottom suspension condition until a complete

* To whom correspondence should be addressed

suspension condition appeared and then reduced slowly. Hosseini et al. (2010) investigated the effect of impeller type, impeller off-bottom clearance, agitation speed, particle size, and particle specific gravity on the mixing quality of sinking particles through numerical simulation and experimental method. Simulation results of the impeller torque and just suspended agitation speed agreed well with experimental values. Tamburini et al. (2011; 2012) reviewed the simulation methods to estimate the just off-bottom agitation speed of glass ballotini particles in water, and presented a universal CFD method. Liu and Barigou (2013) investigated the effect of solid concentration on the liquid velocity field by simulation. They found that the solid concentration of coarse glass particles had little effect on the liquid velocity field when it ranged below 0.1 g/g. As the solid concentration continued to increase, the liquid velocities near the impeller and along the wall of the vessel reduced significantly.

The mixing and dispersing of floating particles is as common as that of sinking particles in the process industry. But there is a large difference between these two processes. The latter process raises the sinking particles whose density is larger than the liquid phase; the former process draws down and disperses the low-density solids floating on the surface (Khazam and Kresta, 2008; Mersmann et al., 1998). The fluctuation of the free surface and eccentric vortex make the motion of floating particles more complex. However, literature on the numerical simulation of the mixing and dispersing of floating particles is relatively scarce. Waghmare et al. (2011) developed a semi-empirical correlation to predict the drawdown rate of floating particles through a conjunction of simulation and experimental measurement. The drawdown rate is correlated to the mean liquid velocity of the free surface. Li et al. (2014) simulated both the solid-liquid mixing of floating particles and sinking particles, which had a great difference in the suspension characteristics. The concentration of sinking particles decreased along with the height while that of floating particles was the opposite. Qiao et al. (2014) compared the effects of up-pumping and down-pumping impellers on the mixing and dispersing of polyethylene particles in water. Other scholars investigated the effects of different material parameters and/or stirred vessel structures on the floating particles mixing with the aid of experiments (Guida et al., 2009; Karcz and Mackiewicz, 2007; 2009; Ozcan-Taskin, 2006; Wojtowicz, 2014).

The existing researches on the mixing and dispersing of floating particles used water as the liquid phase and lost sight of the influence of liquid viscosity. However, viscous materials are commonly adopted inthe actual production. This paper studies the mixing and dispersing of floating particles in a viscous system. Three common impellers were chosen to investigate the effect of impeller type on the solid-liquid mixing by numerical simulation.

PHYSICAL MODEL AND EXPERIMENTAL METHODOLOGY

As shown in Figure 1, a stirred vessel of 380 mm inner diameter (T) and 456 mm liquid level height (H) with a standard elliptical head was adopted. A single baffle of 38 mm breadth (B), 10 mm thickness (d), and 7.6 mm clearance to the vessel wall ($c = T/50$) was fitted in the vessel. A down-pumping propeller (TXL), a six flat-blade disc turbine (Rushton), or a down-pumping six 45° pitched-blade turbine (PBTD-6), as shown in Figure 2, corresponding to axial flow, radial flow and mixed flow impellers, respectively, were adopted in the investigation. The three impellers have the same diameter (D) of 200 mm, agitation speed (N) of 150 rpm, and impeller submergence of 95 mm ($S = T/4$). The vessel structure and agitation speed were determined on account of previous experiments (Chen, 2015). Malt syrup and polyethylene particles were selected as the liquid and solid phases, whose physical parameters are listed in Table 1.

To certify the reliability of simulations, the corresponding experiments were conducted with the same structure, agitation speed, and working medium with simulations. The agitation speed (N) was adjusted by a frequency converter. The shaft torque (M) and system viscosity (μ) were measured by a TQ-660 torque sensor and digital viscometer, respectively. The power number (N_P) and Reynolds number (Re) were calculated by equations (1) and (2).

$$N_P = \frac{P}{\rho N^3 D^5} = \frac{2\pi N\left(M - M_0\right)}{\rho N^3 D^5} = \frac{2\pi\left(M - M_0\right)}{\rho N^2 D^5} \tag{1}$$

$$Re = \frac{\rho N D^2}{\mu} \tag{2}$$

The solid concentrations were sampled by a peristaltic pump.

MATHEMATICAL MODEL AND SIMULATION METHOD

Governing equations

The common models for the simulation of solid-liquid mixing include the Euler-Lagrange model and the Euler-Euler model. The Euler-Lagrange model regards the liquid phase and solid phase as the continuous phase and dispersed phase, respectively. The continuous phase is treated in an Eulerian framework, and the motion of the dispersed phase

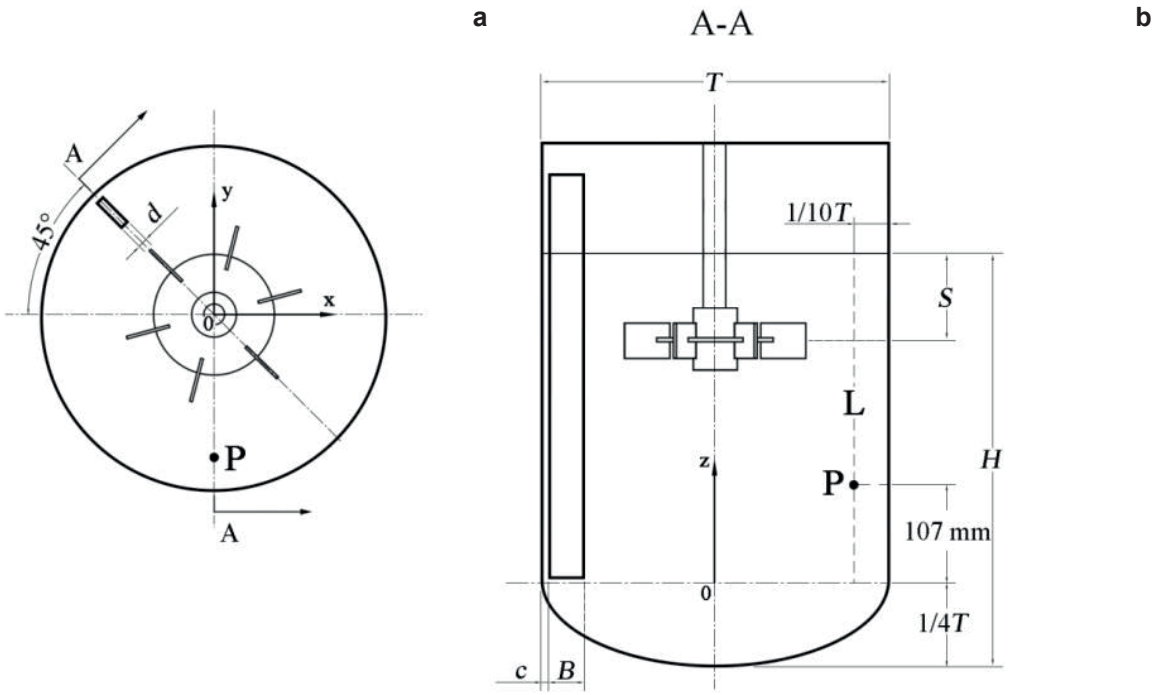

Figure 1. Dimensions of the stirred vessel: (a) Top view; (b) Front view; **L**-Sampling line; **P**-Sampling point.

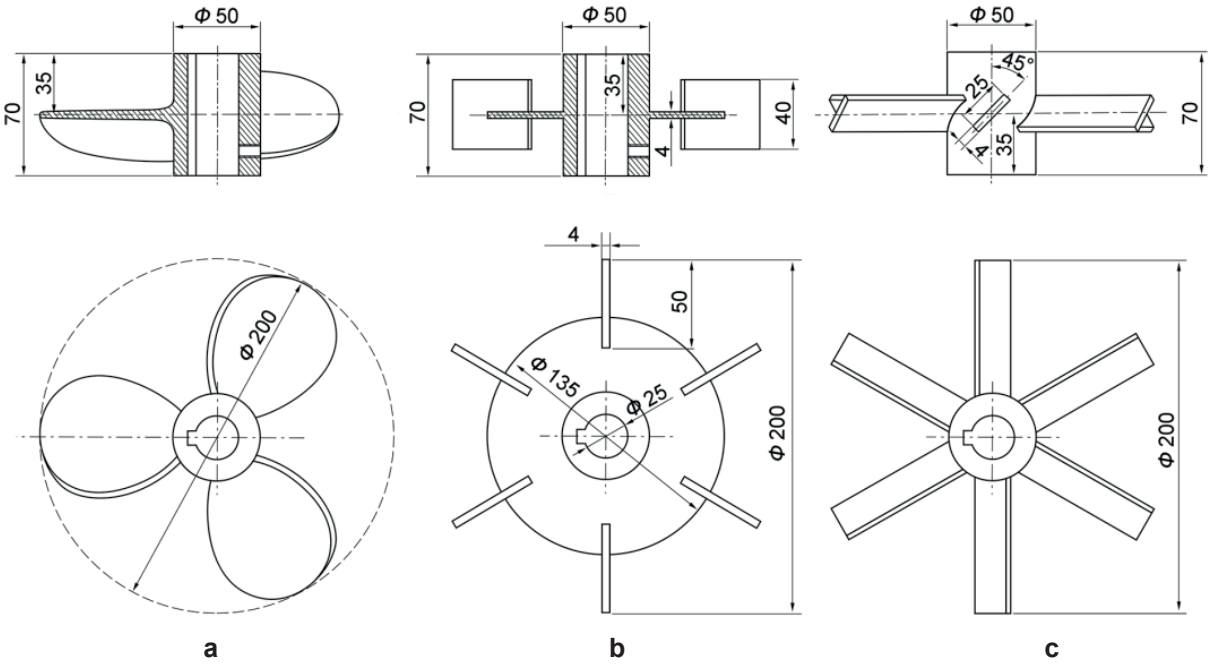

Figure 2. The structures and dimensions of the three impellers: (a) TXL; (b) Rushton; (c) PBTD-6.

Table 1. Physical parameters of the materials.

Physical parameters	Value		Unit
Syrup viscosity (μ_l)	27.3	75.3	mPa·s
Syrup density (ρ_l)	1212.79	1275.6	kg·m^{-3}
Particle density (ρ_s)	831.34		kg·m^{-3}
Particle size	0.7		mm
Mean solid concentration (C_0)	0.05		L/L

is simulated by solving the force balance of each particle. The approach based on this model can obtain more details on the trajectory of the particles when the solid concentration is low. However, with increasing volume fraction of the dispersed phase, the interaction between the two phases increases. It will consume a large sum of computer resources by tracing a large number of particles (Ochieng et al., 2010; Shah et al., 2015). To reduce the computational cost, most researches adopt the Euler-Euler model in the simulation of solid-liquid mixing (Fan et al., 2005; Kasat et al., 2008; Li et al., 2014; Liu et al., 2013; Hosseini et al., 2010; Qiao et al., 2014; Tamburini et al., 2011). The Euler-Euler model is also known as the two-fluid model, which regards both the solid and liquid phases as continuous phases. It is widely used for solid-liquid, gas-liquid and gas-liquid-solid mixing simulation for its own advantages. The simulation results obtained by this method agree well with the corresponding experimental data (Hosseini et al., 2010). Hence, the Euler-Euler model was adopted to simulate the solid-liquid mixing of floating particles in this paper.

In the current simulation, the influence of temperature and reaction was neglected. The governing equations include the continuity equation and momentum conservation equation.

Continuity equation

$$\frac{\partial}{\partial t}\left(\alpha_i \rho_i\right)+\nabla\left(\alpha_i \rho_i \vec{v}_i\right)=0\,,\ \ \sum \alpha_i = 1 \tag{3}$$

Momentum conservation equation

$$\frac{\partial}{\partial t}(\alpha_i \rho_i \vec{v}_i) + \nabla(\alpha_i \rho_i \vec{v}_i \vec{v}_i) = -\alpha_i \nabla p + \nabla \bar{\bar{\tau}}_i + \sum \vec{R}_{ij} + \alpha_i \rho_i \vec{F}_i \tag{4}$$

with

$$\bar{\bar{\tau}}_i = \alpha_i \mu_i (\nabla \vec{v}_i + \nabla \vec{v}_i^T) + \alpha_i \left(\lambda_i - \frac{2}{3}\mu_i\right) \nabla \vec{v}_i \bar{\bar{I}} \tag{5}$$

where i denotes the phase, $i = s$ for the solid phase and $i = l$ for the liquid phase; α_i, ρ_i, and $\vec{v}_i$ are the volume fraction, density, and velocity vector for each phase, respectively; p is the pressure for all the phases; $\bar{\bar{I}}$ is the unit stress tensor; $\vec{F}_i$ is the external body force; $\bar{\bar{\tau}}_i$ is the stress-strain tensor; $\vec{R}_{ij}$ is the interaction force between phases; μ_i and λ_i are the shear viscosity and bulk viscosity for each phase (Jiang and Huang, 2010).

For the solid-liquid two-phase flow, especially in the viscous system, the drag force between phases plays a major role compared with the force between particles (Jiang and Huang, 2010). Hence, equation (6) was taken to calculate the interaction force between phases.

$$\sum \vec{R}_{ij} = \sum K_{ij}\left(\vec{v}_i - \vec{v}_j\right) \tag{6}$$

$$K_{sl} = \frac{\alpha_s \rho_s f}{\tau_s} \tag{7}$$

$$\tau_s = \frac{\rho_s d_s^2}{18\mu_l} \tag{8}$$

where K_{ij} is the momentum exchange coefficient between phases; f is the function of drag force; τ_s is the particle relaxation time; d_s is the diameter of solid particles.

The common drag models used to calculate the momentum exchange coefficient K_{ij} include the Syamlal-O'Brien model, the Wen-Yu model, the Gidaspow model, and so on. The Gidaspow model is the combination of the Wen-Yu model and the Ergun equation (Jiang and Huang, 2010). Based on the previous numerical tests and pertinent literature, the Gidaspow model was taken to calculate the momentum exchange coefficient (Chen, 2015). When α_l is greater than 0.8, the momentum exchange is calculated by equation (9) as below:

$$K_{sl} = \frac{3}{4} C_D \frac{\alpha_s \alpha_l \rho_l \left|\vec{v}_s - \vec{v}_l\right|}{d_s} \alpha_l^{-2.65} \tag{9}$$

Here the drag coefficient C_D is calculated by equation (10).

$$C_D = \frac{24}{\alpha_l Re_s}\left[1 + 0.15\left(\alpha_l Re_s\right)^{0.687}\right] \tag{10}$$

The relative Reynolds number Re_s is defined as below:

$$Re_s = \frac{\rho_l d_s \left|\vec{v}_s - \vec{v}_l\right|}{\mu_l} \tag{11}$$

When α_l does not exceed 0.8, the momentum exchange coefficient is calculated by equation (12):

$$K_{sl} = 150\frac{\alpha_s\left(1-\alpha_l\right)\mu_l}{\alpha_l d_s^2} + 1.75\frac{\rho_l \alpha_s \left|\vec{v}_s - \vec{v}_l\right|}{d_s} \tag{12}$$

Solid phase pressure estimated for the granular flows (whose volume fraction is lower than the maximum allowable value) used to calculate the term ∇p_s is composed of a kinetic term and a second term as follows (Jiang and Huang, 2010):

$$p_s = \alpha_s \rho_s \Theta_s + 2\rho_s\left(1+e_{ss}\right)\alpha_s^2 g_{0,ss}\Theta_s \tag{13}$$

The shear viscosity μ_s and bulk viscosity λ_s of the solid phase in equation (5) can be calculated as follows:

$$\mu_s = \mu_{s,\mathrm{col}} + \mu_{s,\mathrm{kin}} \tag{14}$$

$$\mu_{s,\mathrm{col}} = \frac{4}{5}\alpha_s^2 \rho_s d_s g_{0,ss}\left(1+e_{ss}\right)\left(\frac{\Theta_s}{\pi}\right)^{1/2} \tag{15}$$

$$\mu_{s,\mathrm{kin}} = \frac{10\rho_s d_s\sqrt{\Theta_s \pi}}{96\left(1+e_{ss}\right)g_{0,ss}}\left[1+\frac{4}{5}g_{0,ss}\alpha_s\left(1+e_{ss}\right)\right]^2 \tag{16}$$

$$\lambda_s = \frac{4}{3}\alpha_s^2 \rho_s d_s g_{0,ss}\left(1+e_{ss}\right)\left(\frac{\Theta_s}{\pi}\right)^{1/2} \tag{17}$$

where Θ_s is the granular temperature; e_{ss} is the restitution coefficient for particle collision; $g_{0,ss}$ is the radial distribution function; $\mu_{s,\mathrm{col}}$ and $\mu_{s,\mathrm{kin}}$ are the collisional and kinetic viscosity of the solid phase. The granular temperature conservation equation based on the kinetic theories takes the following form (Jiang and Huang, 2010):

$$\frac{3}{2}\left[\frac{\partial}{\partial t}\left(\rho_s \alpha_s \Theta_s\right) + \nabla\cdot\left(\rho_s \alpha_s \vec{v}_s \Theta_s\right)\right] = \left(-p_s\bar{\bar{I}} + \bar{\bar{\tau}}_s\right):\nabla\vec{v}_s + \nabla\cdot\left(k_{\Theta_s}\nabla\Theta_s\right) - \gamma_{\Theta_s} + \Phi_{ls} \tag{18}$$

where $\left(-p_s\bar{\bar{I}}+\bar{\bar{\tau}}_s\right)\nabla\vec{v}_s$ is the generation of energy by the solid stress tensor; $k_{\Theta_s}\nabla\Theta_s$ is the diffusion of energy; k_{Θ_s} is the diffusion coefficient; γ_{Θ_s} is the collisional dissipation of energy; Φ_{ls} is the energy exchange between the fluid phase *l* and the solid phase *s*. The term γ_{Θ_s} is represented by Lun et al. (1984):

$$\gamma_{\Theta_s}=\frac{12\left(1-e_{ss}^2\right)g_{0,ss}}{d_s\sqrt{\pi}}\rho_s\alpha_s^2\Theta_s^{3/2} \tag{19}$$

The term Φ_{ls} is represented as follow:

$$\Phi_{ls}=-3K_{ls}\Theta_s \tag{20}$$

Turbulence model

Comparing with the other two extensions of the standard *k-ε* turbulence model (dispersed and per-phase), the mixture *k-ε* model has less computational demand and better representation of the solid distribution (Qiao et al., 2014). Hence, it was adopted as the turbulence model for simulation in this paper. The equations are listed as below.

$$\frac{\partial}{\partial t}(\rho_m k)+\nabla\cdot(\rho_m\vec{v}_m k)=\nabla\cdot\left(\frac{\mu_{t,m}}{\sigma_k}\nabla k\right)+G_{k,m}-\rho_m\varepsilon \tag{21}$$

$$\frac{\partial}{\partial t}(\rho_m\varepsilon)+\nabla\cdot(\rho_m\vec{v}_m\varepsilon)=\nabla\cdot\left(\frac{\mu_{t,m}}{\sigma_\varepsilon}\nabla\varepsilon\right)+\frac{\varepsilon}{k}\left(C_{1\varepsilon}G_{k,m}-C_{2\varepsilon}\rho_m\varepsilon\right) \tag{22}$$

where *k* is the turbulent kinetic energy; *ε* is the turbulent kinetic energy dissipation rate; $\mu_{t,m}$ is the turbulent viscosity; $G_{k,m}$ is the generation of turbulence in the mixture. The mixture density (ρ_m) and mixture velocity ($\vec{v}_m$) are calculated by equations (23) to (24) (Jiang and Huang, 2010).

$$\rho_m=\sum_{i=1}^{N}\alpha_i\rho_i \tag{23}$$

$$\vec{v}_m=\frac{\sum_{i=1}^{N}\alpha_i\rho_i\vec{v}_i}{\sum_{i=1}^{N}\alpha_i\rho_i} \tag{24}$$

Simulation method

The commercial CFD software FLUENT was utilized for the numerical simulation of the solid-liquid mixing of floating particles. The multiple reference frame method (MRF) was applied to calculate the flow field, which divided the whole vessel into moving area and static area. The moving area consisted of a central cylinder region with the entire impeller area, which used a rotating reference frame with the agitation speed. Other regions were defined as the static area with static reference frame. No-slip boundary conditions with the standard wall function were imposed on the solid walls for the liquid phase. Partial-slip boundary condition (Johnson and Jackson, 1987) was considered for the solid phase.The solid walls included the vessel wall, the surface of the baffle, impeller and shaft. The symmetry boundary condition was imposed on the free liquid surface. The interface boundary condition was imposed on the interface between the moving and static areas.

The second order upwind scheme was used for the momentum, turbulent kinetic energy, and turbulent dissipation rate. The phase coupled SIMPLE algorithm was adopted for the pressure-velocity coupling. The time step was set to 0.001 s. The residual criterion for convergence of the flow field and concentration field were 10^{-6} and 10^{-8}, respectively. The addition of a second phase employed the method of patch in initialization. The floating particles with an initial volume fraction of 0.05 L/L were uniformly distributed in the liquid phase.

Mesh generation

The models were meshed by the CFD pre-processing software GAMBIT. The moving area around the impeller and the static elliptical head region were meshed with the unstructured tetrahedral element because of their

irregularity. Other regions were meshed with the structured hexahedral element. Local grids around the impeller were refined in addition. The specific mesh is shown in Figure 3.

Establishing adequacy of computational grids is important for the numerical simulation. The appropriate mesh quantity will save the computer resource, improve the computing speed, and ensure the accuracy. Based on the grid independence test, we increased the number of grids by the factor of 2 until the turbulence intensity stop changing. The appropriate grid numbers of the three stirred vessels are listed in Table 2.

RESULTS AND DISCUSSION

Effect of boundary condition for the solid phase

Specularity coefficient (Φ) is an empirical parameter to qualify the particle-wall collisions in partial-slip boundary condition, whose range is from 0 to 1 (Li et al., 2010). The smaller coefficient corresponds to a smoother wall with less friction. It is hard to obtain the specularity coefficient through an experimental method. Data simulated on the sampling line L shown in Figure 1 in a stirred vessel equipped with a TXL impeller under four different boundary conditions for the solid phase, were compared in Figure 4. The first condition corresponded to the no-slip boundary condition, while the other three corresponded to partial-slip boundary conditions with specularity coefficient of 0, 0.5, and 1. The impeller speed, liquid viscosity, and mean solid concentration were 150 rpm, 75.3 mPa·s and 0.05 L/L, respectively. It can be concluded that the effect of specularity coefficient on the liquid velocity, turbulence intensity, and solid concentration can be neglected in this study. Compared with the other region, the area near the solid wall was very small. The motions of the solid particles were controlled by the flow pattern of the liquid phase. Hence, the effect of the boundary condition for the solid phase was quite limited. In fact, most research on the simulation of solid-liquid mixing adopted the no-slip boundary condition on the wall for the solid phase instead of the partial-slip boundary condition (Fan et al., 2005; Hosseini et al., 2010; Qiao et al., 2014; Tamburini et al., 2012; Waghmare et al., 2011). In the remaining sections of this paper, the partial-slip boundary condition with a specularity coefficient of 0 was adopted as the wall condition for the solid phase.

Simulation reliability verification

The power curve of the TXL impeller in a system of 27.3 mPa·s viscosity simulated with the Gidaspow model was compared with the experimental result in Figure 5. The maximum and minimum errors between simulation and experiment are 18.0% and 8.59%, respectively.

Furthermore, Figure 6 shows the dimensionless solid concentrations (C/C_0) of the sampling point P1 shown in Figure 1 obtained by simulation and experiment. The dimensionless solid concentrations with the agitation speed lower than 80 rpm are close to 0. Hence, the data errors are relatively large. Leaving out the first three experimental data, the maximum error between simulation and experiment was 24.3% at an agitation speed of 90 rpm.

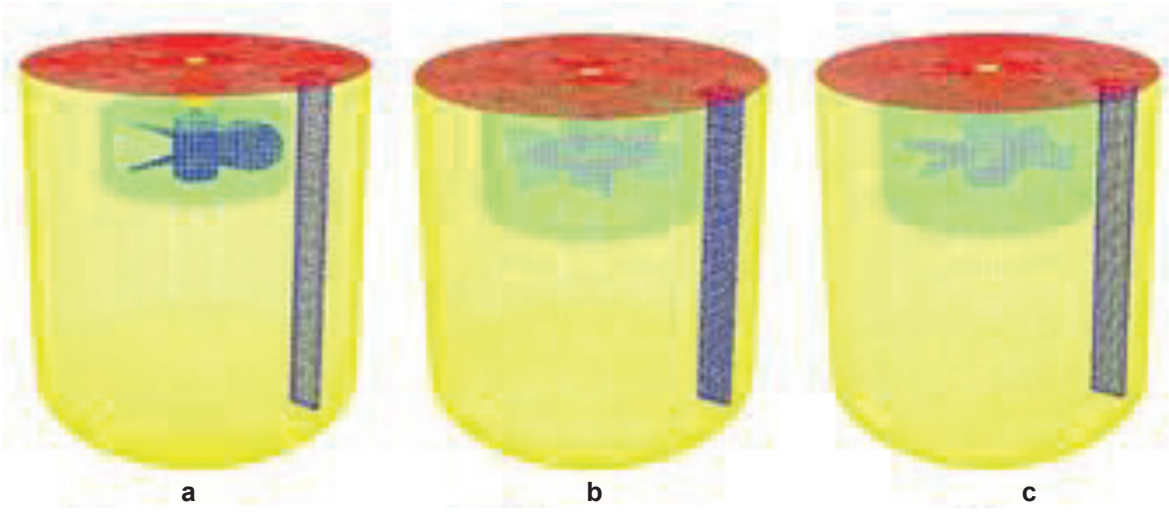

Figure 3. Discretization of stirred vessels: (a) TXL; (b) Rushton; (c) PBTD-6.

Table 2. Grid numbers of the stirred vessels equipped with different impellers.

Impeller type	TXL	Rushton	PBTD-6
Grid number	345720	357952	376164

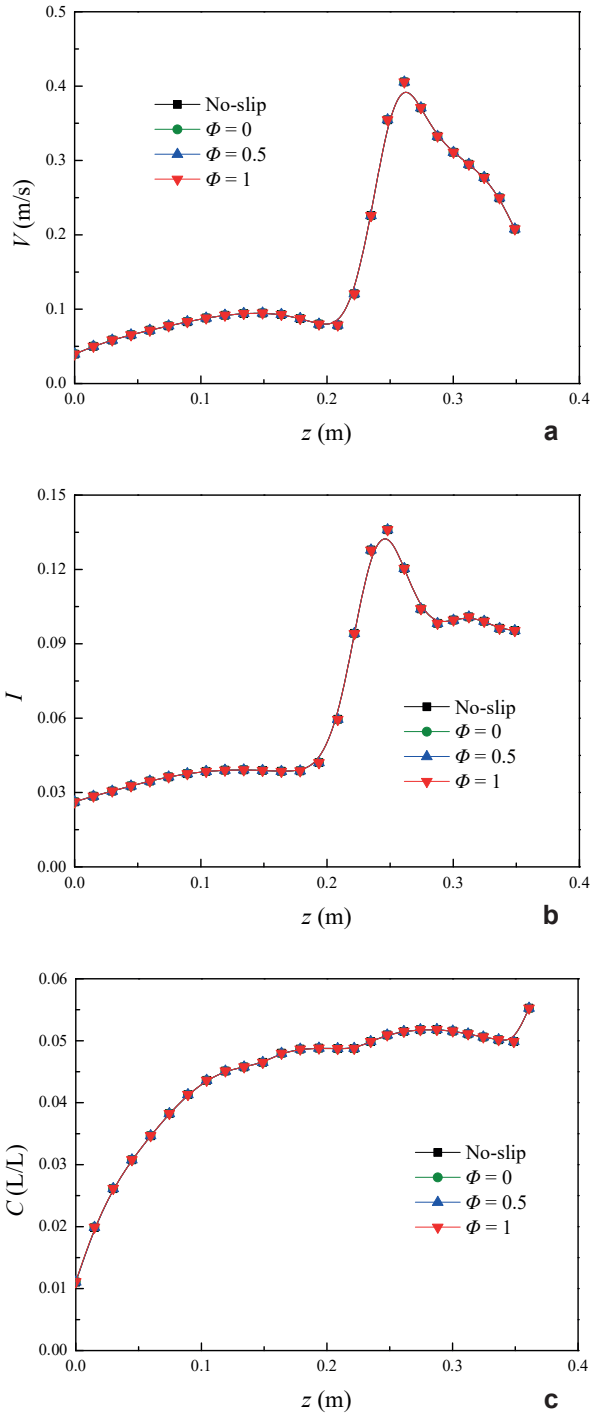

Figure 4. Comparison of different boundary conditions for the solid phase on the sampling line L shown in Figure 1 (TXL, N = 150 rpm, μ = 75.3 mPa·s, C_0 = 0.05 L/L): (a) Liquid velocity; (b) Turbulence intensity; (c) Solid concentration.

The minimum error was 1.97% at an agitation speed of 110 rpm. This verifies the Gidaspow model and other settings are suitable for the simulation of solid-liquid mixing with floating particles, which can also provide a basis and support for the follow-up simulation.

Distribution of liquid velocity field

The distributions of liquid velocity field in a system of 75.3 mPa·s viscosity in the vessel equipped with a TXL impeller, a Rushton turbine, and a PBTD-6 turbine were investigated by simulation and shown in Figure 7. In addition, liquid velocities on a radius in the three vessels are compared in Figure 8. As shown in Figure 1, the coordinate origin was located at the center of the elliptical head; the z-axis was upward along the symmetry axis of the stirred vessel. The radius is 1 mm under the liquid surface where z = 360 mm shown in Figure 7.

Figure 7 shows that the radial flow was developed around the impeller when the Rushton turbine was adopted. The fluid was divided into two streams near the vessel wall: one stream flowed upward, converged to the center in a spiral way near the surface to generate a surface vortex, and flowed down to the turbine; another stream flowed downward, converged to the center at the bottom of the vessel, and flowed upward along the axis. When a PBTD-6 turbine was adopted, the liquid flowed with a downward bias under the effect of blades, and was divided into two streams upward and downward near the wall.

As shown in Figure 8, (1) the average axial, radial, and tangential liquid velocities on the radius near the surface in the vessel equipped with a TXL impeller were smaller than those in the vessels equipped withthe other two impellers at the agitation speed of 150 rpm. This means that higher agitation speed was required to draw down and disperse the solids with a TXL impeller. (2) The maximum tangential liquid velocities near the surface of the vessels equipped with a TXL impeller, a Rushton turbine, or a PBTD-6 turbine are 0.366 m/s, 0.777 m/s, and 0.433 m/s, respectively. The tangential liquid velocity in the vessel equipped with a Rushton turbine was nearly twice as much as those corresponding to the other two impellers. For the Rushton turbine, the normal direction of the blade was the same with the linear velocity direction of the impeller. Hence, the force of the blade acting on the liquid was stronger than that of the TXL impeller and PBTD-6 turbine.

Distribution of turbulence intensity

High turbulence intensity is beneficial to increase the rate of drawdown and dispersing for solids in the stirred vessel. The distributions of turbulence intensity caused by the TXL impeller, Rushton turbine, and PBTD-6 turbine were investigated in the system with 75.3 mPa·s viscosity, which are shown in Figure 9.

As seen in Figure 9, (1) the turbulence intensity around the impeller was larger than those of the other regions in the vessel. The turbulence intensity on the blade tip of the impeller was the largest. This is because the linear velocity ofthe blade tip was the highest. The trailing vortexes generated behind the blades would also enhance the turbulence of fluid. (2) The turbulence intensity on the

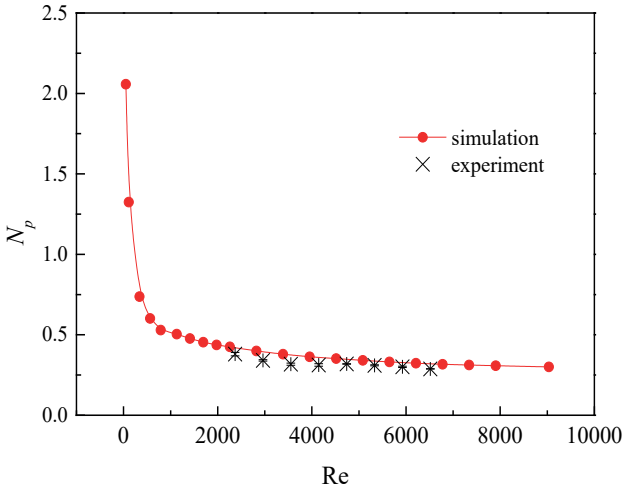

Figure 5. Numerical and experimental (error bar with standard deviation) power curve (TXL, μ = 27.3 mPa·s, C_0 = 0.05 L/L).

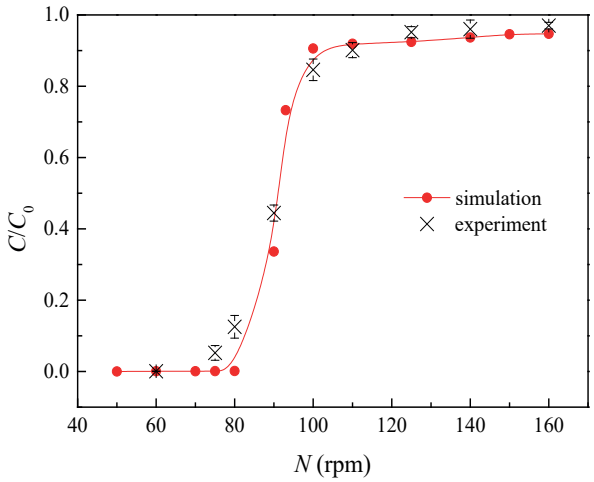

Figure 6. Numerical and experimental (error bar with standard deviation) dimensionless solid concentrations of the sampling point P1 shown in Figure 1 (TXL, μ = 27.3 mPa·s, C_0 = 0.05 L/L).

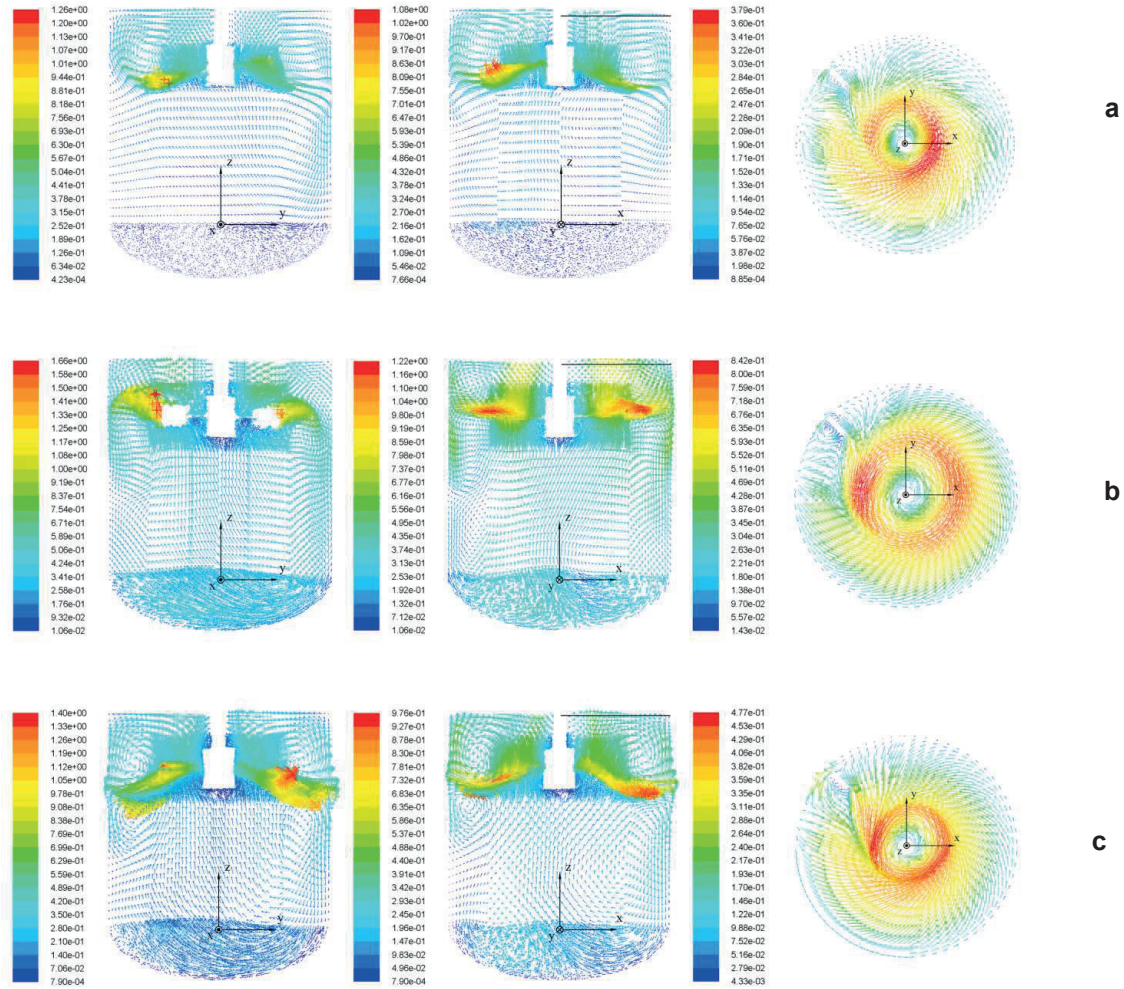

Figure 7. Liquid velocity (m/s) field distribution in the *y*-*z* plane (x = 0), *x*-*z* plane (y = 0), and *x*-*y* plane (z = 361mm) corresponding to different impellers (N = 150 rpm, μ = 75.3 mPa·s, C_0 = 0.05 L/L): (a) TXL; (b) Rushton; (c) PBTD-6.

azimuth of 90° behind the baffle near the agitation shaft on the surface was relatively large for all three impellers

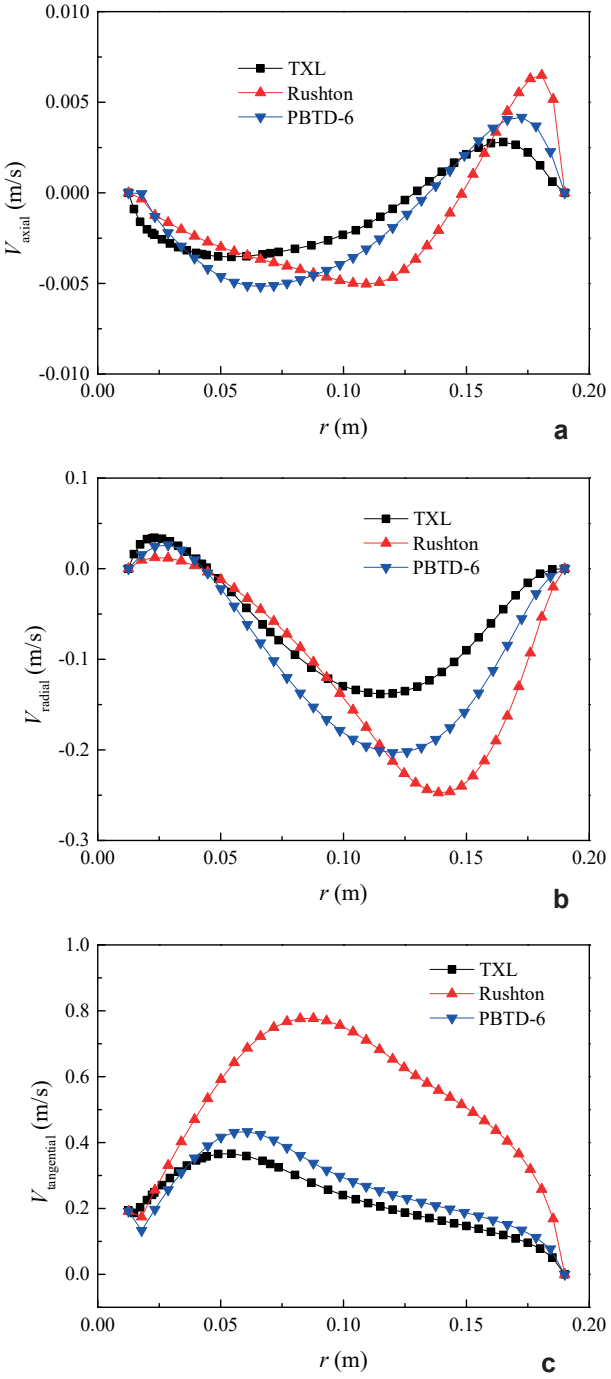

Figure 8. Comparison of the liquid velocity on a radius 1mm under the liquid surface shown in Figure 7 corresponding to different impellers (N = 150 rpm, μ = 75.3 mPa·s, C_0 = 0.05 L/L): (a) Axial velocity; (b) Radial velocity; (c) Tangential velocity.

in the vessel equipped with a single baffle. As affected by the baffle, the tangential flow near the wall flowed to the center radially. It was mixed with the tangential flow near the center and generated the eccentric vortex. The position of the vortex observed in experiment (Liu et al., 2016), as shown in Figure 10, was basically the same where the largest intensity appeared in the simulation (Chen, 2015). (3) The turbulence intensity near the surface in the vessel equipped with a Rushton turbine was larger than those in the vessels equipped with other impellers. As shown in Figure 7 and Figure 8, the liquid velocity near the surface in the vessel equipped with a Rushton turbine was relatively larger. Higher velocity resulted in stronger turbulence intensity.

Distribution of solid concentration field

The distribution of solid concentration field is an important index to evaluate the performance of solid-liquid mixing. Usually, it is hard to obtain the entire concentration distribution in the vessel by experiment. However, it can be visually displayed by simulation, which is beneficial to enhance the understanding of solid-liquid mixing. The distributions of solid concentration field in vessels equipped with a TXL impeller, a Rushton turbine, and a PBTD-6 turbine were investigated by simulation.

Figure 11 shows that, (1) particles tend to accumulate on the surface around the agitation shaft in the three vessels during steady-state conditions. As seen in Figure 7, the liquid on the surface converged to the center in a spiral way with particles carried. So particles concentrated to the center of the liquid surface. (2) The uniformity of the vessel equipped with a TXL impeller was the worst of the three at the same agitation speed of 150 rpm. The literature (Chen, 2015) indicates that the just drawdown speed (N_{jd}) of the TXL impeller was higher than those of the Rushton and the PBTD-6 turbines. The working speed of 150 rpm was much closer to the critical speed of the Rushton turbine. The just drawdown speed of the TXL impeller in these conditions was nearly 160 rpm; consequently, it was hard to draw down and disperse the floating particles on the surface at the agitation speed of 150 rpm which was lower than the just drawdown speed. The simulation result shows that the TXL impeller needs a higher speed than the other two impellers to reach a just drawdown state, which was in consonance with the experimental results. (3) The distribution of particles in the stirred vessel was not symmetric and had a certain offset relative to the axis. The structural asymmetry of the stirred vessel with a single baffle resulted in an eccentric vortex and flow asymmetry in the vessel. It led to an asymmetry of solid concentration in the vessel.

Solid concentrations on the sampling line L shown in Figure 1 and Figure 11 for the three impellers are compared in Figure 12. The degrees of homogeneity for the three vessels were represented by the standard deviation (σ) defined as equation (25) (Bohnet and Niesmak, 1979).

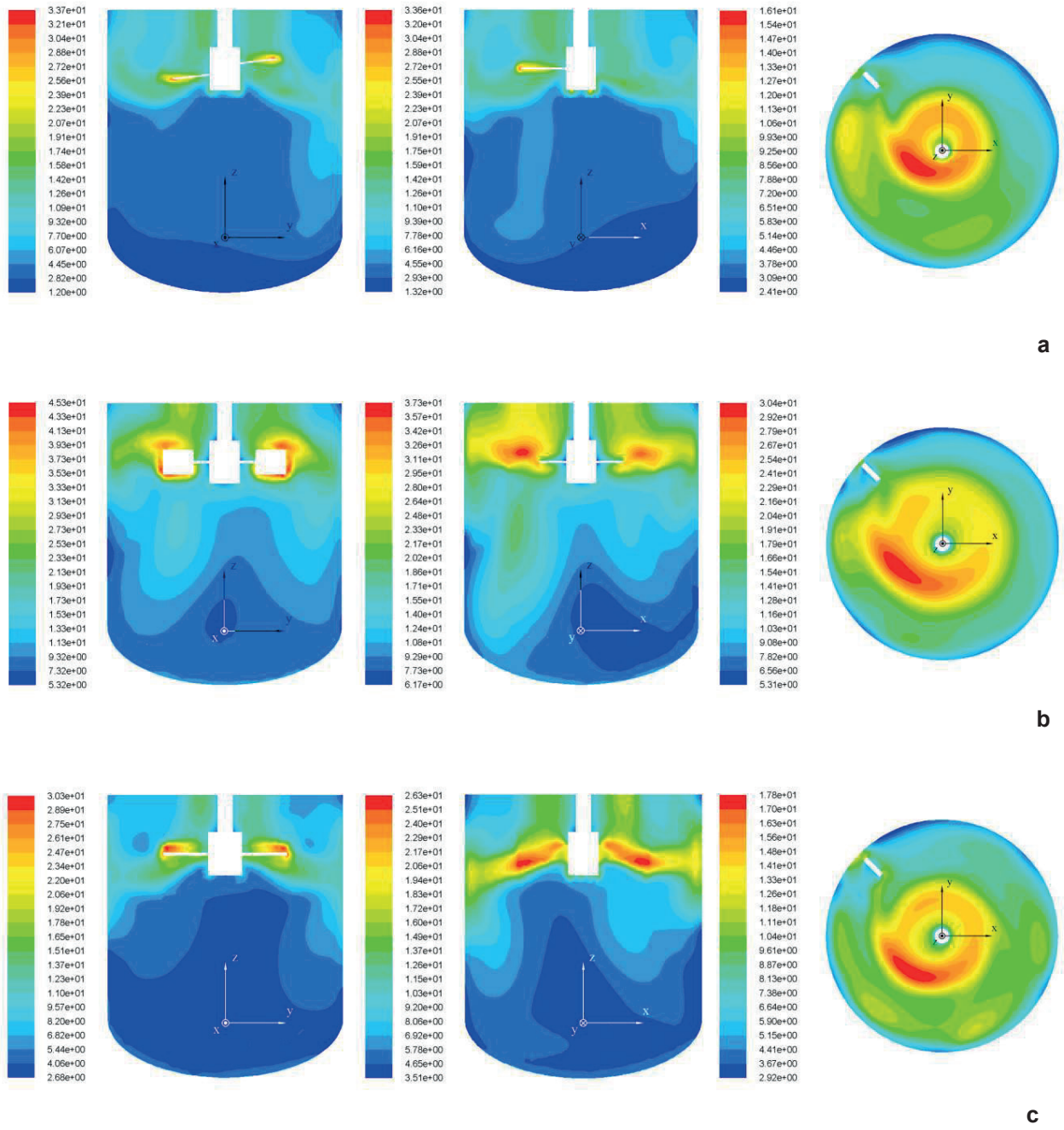

Figure 9. Turbulence intensity (%) distribution in the *y*-*z* plane ($x = 0$), *x*-*z* plane ($y = 0$), and *x*-*y* plane ($z = 361$ mm) corresponding to different impellers ($N = 150$ rpm, $\mu = 75.3$ mPa·s, $C_0 = 0.05$ L/L): (a) TXL; (b) Rushton; (c) PBTD-6.

$$\sigma = \sqrt{\frac{1}{n}\sum_{1}^{n}\left(\frac{C}{C_0} - 1\right)^2} \qquad (25)$$

The standard deviations for the three vessels equipped with a TXL impeller, a Rushton turbine, or a PBTD turbine were 0.242, 0.0275, and 0.0334, respectively. It can be concluded that, at the same agitation speed of 150 rpm, the homogeneity in the axial direction in the vessel equipped with a Rushton turbine or a PBTD-6 turbine was much better than that in the vessel equipped with a TXL.

CONCLUSIONS

The distributions of velocity, turbulence intensity, and solid concentration in the stirred vessel equipped with a

Figure 10. Eccentric vortex observed in experiment (TXL impeller, $N = 150$ rpm, $\mu = 75.3$ mPa·s, $C_0 = 0.05$ L/L).

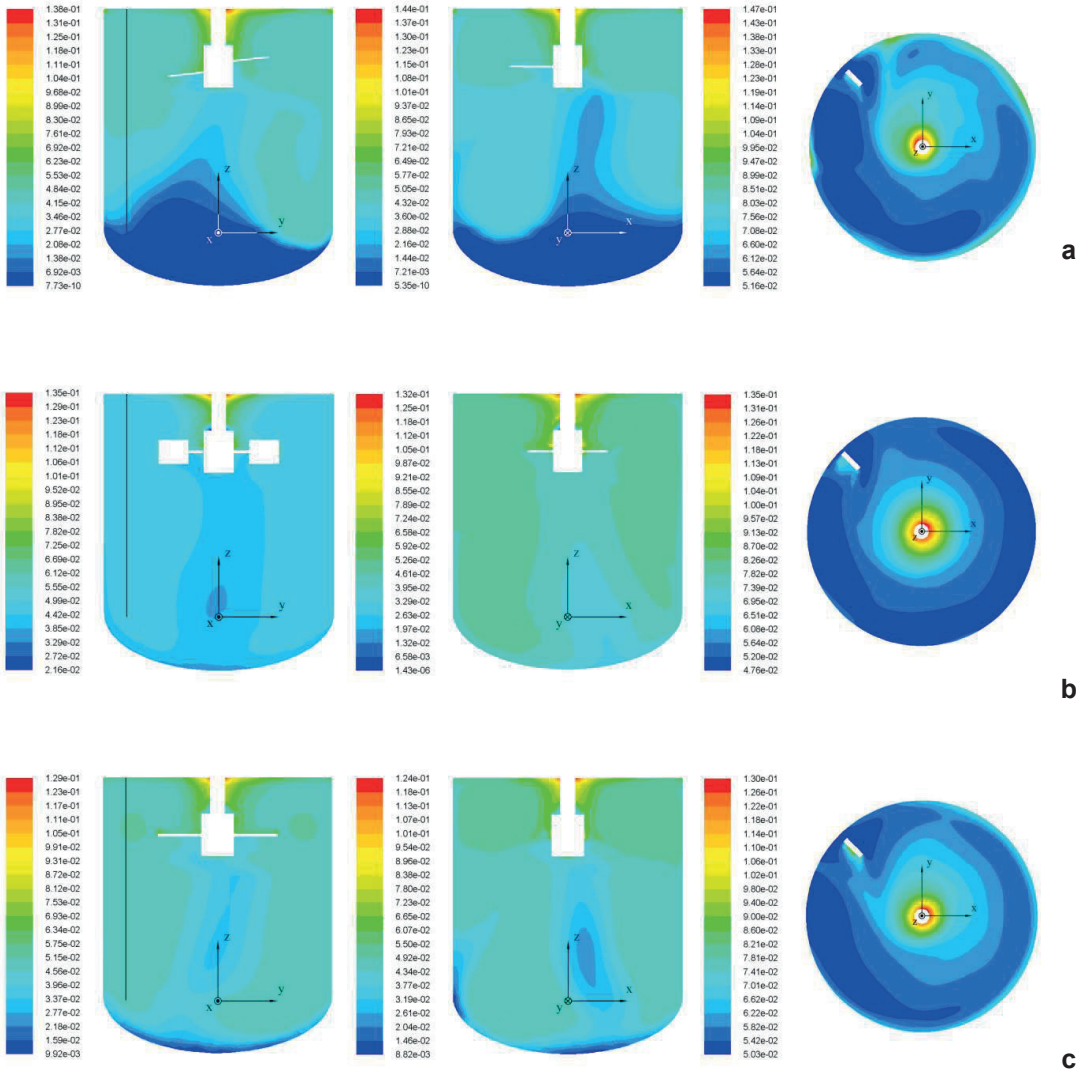

Figure 11. Solid concentration (L/L) field distribution in the *y-z* plane ($x = 0$), *x-z* plane ($y = 0$), and *x-y* plane ($z = 361$ mm) corresponding to different impellers ($N = 150$ rpm, $\mu = 75.3$ mPa·s, $C_0 = 0.05$ L/L): (a) TXL; (b) Rushton; (c) PBTD-6.

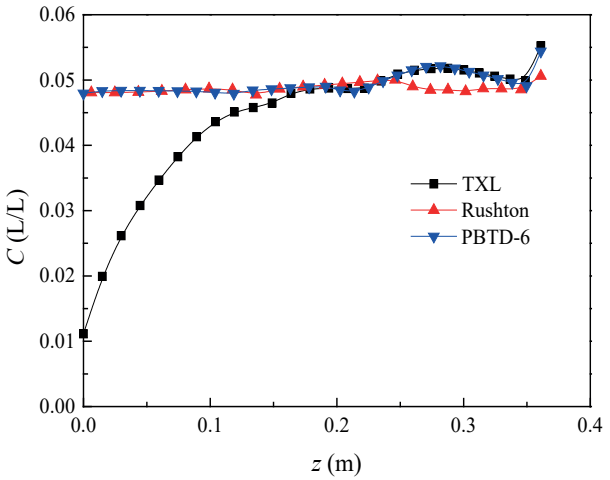

Figure 12. Comparison of the solid concentration on the sampling line L shown in Figure 1 corresponding to different impellers (N = 150 rpm, μ = 75.3 mPa·s, C_0 = 0.05 L/L).

single baffle and a TXL impeller, or a Rushton turbine, or a PBTD-6 turbine were compared by simulation with the help of the Gidaspow model. Three impellers of 200 mm diameter, 95 mm immersion depth and 150 rpm agitation speed were adopted in the simulations. The results showed that:

(1) The power curve of the TXL impellerand the dimensionless solid concentration of the point P1 were obtained by simulation with the Gidaspow model and experiment. It can be confirmed that the Gidaspow drag model is applicable to simulate the solid-liquid mixing process of floating particles in a viscous system by comparing the simulation results andexperimental data.

(2) It is beneficial to generate an eccentric vortex on the azimuth of 90° behind the baffle near the agitation shaft on the surface when the stirred vessel was equipped with a single baffle. The turbulence intensity of this position was found to be relatively larger according to the simulations.

(3) The agitation speed of 150 rpm adopted inthe simulation was much closer to the just drawdown speed of the Rushton turbine. It did not reach the critical state of the TXL impeller. The uniformity of the vessel with a TXL impeller was the worst of the three. The critical speed of the TXL impeller was higher than those of the Rushton turbine and PBTD-6 turbine.

NOMENCLATURE

B	breadth of baffle, mm
c	clearance between baffle and vessel wall, mm
C	solid concentration, L/L
C_D	drag coefficient, mm
C_0	mean solid concentration, L/L
d	thickness of baffle, mm
d_s	diameter of solid particle, mm
D	diameter of impeller, mm
e_{ss}	restitution coefficient
f	function of drag force
$\vec{F}_i$	external body force, N
$g_{0,ss}$	radial distribution function
$G_{k,m}$	turbulence generation, kg/m·s^3
H	liquid level height, mm
I	turbulence intensity
$\bar{\bar{I}}$	unit stress tensor
k	turbulent kinetic energy, m^2/s^2
k_{Θ_s}	diffusion coefficient
K_{ij}	momentum exchange coefficient between phases
K_{sl}	momentum exchange coefficient between solid and liquid
M	shaft torque, N·m
M_0	no-load shaft torque, N·m
N	agitation speed, rpm
N_{jd}	just drawdown speed, rpm
N_P	power number
p	pressure for all phases, Pa
p_s	solid phase pressure, Pa
P	power, W
Re	Reynolds number
Re_s	relative Reynolds number
$\vec{R}_{ij}$	interaction force between phases, N
S	impeller submergence, mm
t	time, s
T	inner diameter of stirred vessel, mm
$\vec{v}_i$	velocity vector of phase i, m/s
$\vec{v}_j$	velocity vector of phase j, m/s
$\vec{v}_l$	velocity vector of liquid phase, m/s
$\vec{v}_m$	mixture velocity, m/s
$\vec{v}_s$	velocity vector of solid phase, m/s
V	liquid velocity, m/s
V_{axial}	axial velocity of liquid, m/s
V_{radial}	radial velocity of liquid, m/s
$V_{tangential}$	tangential velocity of liquid, m/s

Greek letters

α_i	volume fraction of phase i
α_s	volume fraction of solid phase
α_l	volume fraction of liquid phase
γ_{Θ_s}	collisional dissipation of energy, m^2/s^2
ε	turbulent kinetic energy dissipation rate, m^2/s^3
Θ_s	granular temperature, m^2/s^2

λ_i	bulk viscosity of phase *i*, Pa·s
λ_s	bulk viscosity of solid phase, Pa·s
μ	viscosity, Pa·s
μ_i	shear viscosity of phase *i*, Pa·s
μ_l	viscosity of liquid phase, Pa·s
μ_s	shear viscosity of solid phase, Pa·s
$\mu_{s,\mathrm{col}}$	collisional viscosity of solid phase, Pa·s
$\mu_{s,\mathrm{kin}}$	kinetic viscosity of solid phase, Pa·s
$\mu_{t,m}$	turbulent viscosity, Pa·s
ρ_i	density of phase *i*, kg/m^3
ρ_l	density of liquid phase, kg/m^3
ρ_m	mixture density, kg/m^3
ρ_s	density of solid phase, kg/m^3
σ	standard deviation
$\bar{\bar{\tau}}_i$	stress-strain tensor of phase *i*, N/m
τ_s	particle relaxation time, s
Φ	specularity coefficient
Φ_{ls}	energy exchange between the fluid phase *l* and the solid phase *s*, m^2/s^2

Abbreviation

CFD	computational fluid dynamics
MRF	multiple reference frame
PBTD-6	down-pumping six 45° pitched-blade turbine
Rushton	six flat-blade disc turbine
TXL	down-pumping propeller

ACKNOWLEDGMENTS

This work was financially supported by the National Natural Science Foundation of China (21776246) and the Zhejiang Provincial Natural Science Foundation of China (LY16B060003).

REFERENCES

Bohnet, M., and Niesmak, G. Distribution of solids in stirred suspensions. Chemie Ingenieur Technik, 51, No. 4, 314 (1979).

Chen, M. Q., Research on the mechanical mixing of floating particles with high concentration in viscous system. Master Thesis, Zhejiang University (2015).

Fan, L., Mao, Z. and Wang, Y., Numerical simulation of turbulent solid-liquid two-phase flow and orientation of slender particles in a stirred tank. Chemical Engineering Science, 60, 7045 (2005).

Feng, L. F. and Wang, J. J., Reactor. Chemical Industry Press, Beijing (2010).

Guida, A., Fan, X., Parker, D. J., Nienow, A. W. and Barigou, M., Positron emission particle tracking in a mechanically agitated solid-liquid suspension of coarse particles. Chemical Engineering Research and Design, 87, No. 4, 421 (2009).

Hosseini, S., Patel, D., Ein-Mozaffari, F. and Mehrvar, M., Study of solid-liquid mixing in agitated tanks through computational fluid dynamics modeling. Industrial & Engineering Chemistry Research, 49, 4426 (2010).

Johnson, P. C., and Jackson, R. Frictional-collisional constitutive relations for granular materials, with application to plane shearing. Journal of Fluid Mechanics, 176, 67 (1987).

Jiang, F. and Huang, P. The analyses of Fluent advanced applications and examples. Tsinghua University Press, Beijing (2010).

Karcz, J. and Mackiewicz, B., An effect of particles wettability on the draw down of floating solids in a baffled agitated vessel equipped with a high-speed impeller. Chemical and Process Engineering, 28, 661 (2007).

Karcz, J. and Mackiewicz, B., Effects of vessel baffling on the drawdown of floating solids. Chemical Papers, 63, No. 2, 164 (2009).

Kasat, G. R., Khopkar, A. R.,Ranade, V. V. and Pandit, A. B., CFD simulation of liquid-phase mixing in solid-liquid stirred reactor. Chemical Engineering Science, 63, 3877 (2008).

Khazam, O. and Kresta, S. M., Mechanisms of solids drawdown in stirred tanks.Canadian Journal of Chemical Engineering, 86, 622 (2008).

Li, T. W., Zhang, Y. M., Grace, J. R., Bi X. T., Numerical investigation of gas mixing in gas-solid fluidized beds. AIChE Journal, 56, No.9, 2280 (2010).

Li, L. C., Xu, B. and Yang, J., Sinking/floating particles solid suspension characteristics in stirred tank based on CFD simulation. Journal of Mechanical Engineering (Chinese), 50, No. 12, 185 (2014).

Liu, L. and Barigou, M., Numerical modelling of velocity field and phase distribution in dense monodisperse solid-liquid suspensions under different regimes of agitation: CFD and PEPT experiments. Chemical Engineering Science, 101, 837 (2013).

Liu, B., Zheng, Y., Chen, M., Huang, B. and Jin Z., Experimental study on the mixing and dispersing of floating particles in viscous system. Canadian Journal of Chemical Engineering, 94, 2013 (2016).

Lun, C. K. K., Savage, S. B., Jeffrey, D. J. and Chepurniy, N., Kinetic theories for granular flow: inelastic particles in a general flow field. Journal of Fluid Mechanics, 140, 223 (1984).

Mersmann, A., Werner, F., Maurer, S. and Bartosch, K., Theoretical prediction of the minimum stirrer speed in mechanically agitated suspensions. Chemical Engineering and Processing, 37, 503 (1998).

Ochieng, A. and Onyango, A. S., CFD simulation of solids suspension in stirred tanks: review. Hemijska Industrija, 64, No. 5, 365 (2010).

Ozcan-Taskin, G., Effect of scale on the draw down of floating solids. Chemical Engineering Science,61, 2871 (2006).

Qiao, S., Wang, R., Yang, X. and Yan, Y., CFD prediction of effects of impeller design on floating solids mixing in stirred tanks with pitched blade turbines. Journal of Chemical Engineering of Japan, 47, No.5, 373 (2014).

Rajavathsavai, D., Khapre, A. and Munshi, B., Study of mixing behavior of CSTR using CFD. Brazilian Journal of Chemical Engineering, 31, No. 1, 119 (2014).

Shah, R. S. S. R. E., Sajjadi, B., Raman, A. A. A. and Ibrahim, S., Solid-liquid mixing analysis in stirred vessels. Reviews in Chemical Engineering, 31, No. 2, 119 (2015).

Tamburini, A., Cipollina, A., Micale, G., Brucato, A. and Ciofalo, M., CFD simulations of dense solid-liquid suspensions in baffled stirred tanks: predictions of suspension curves. Chemical Engineering Journal, 178, 324 (2011).

Tamburini, A., Cipollina, A., Micale, G., Brucato, A. and Ciofalo, M., CFD simulation of dense solid-liquid suspensions in baffled stirred tanks: prediction of the minimum impeller speed for complete suspension. Chemical Engineering Journal, 193, 234 (2012).

Tamburini, A., Cipollina, A., Micale, G. and Brucato, A., Particle distribution in dilute solid liquid unbaffled tanks via a novel laser sheet and image analysis based technique. Chemical Engineering Science, 87, 341 (2013).

Waghmare, Y., Falk,R., Graham,L. and Koganti, V., Drawdown of floating solids in stirred tanks: scale-up study using CFD modeling. International Journal of Pharmaceutics, 418, 243 (2011).

Wang, K. and Feng, L. F., Mixing equipment design. China Machine Press, Beijing (2000).

Wojtowicz, R., Choice of an optimal agitated vessel for the drawdown of floating solids. Industrial & Engineering Chemistry Research, 53, 13989 (2014).

Wu, B. X., CFD simulation of mixing for high-solids anaerobic digestion. Biotechnology and Bioengineering, 109, No. 8, 2116 (2012).